

## Electronic Supplementary Information

### **Achieving 11.95% efficient $\text{Cu}_2\text{ZnSnSe}_4$ solar cells fabricated by sputtering Cu-Zn-Sn-Se quaternary compound target with selenization process**

Xinchen Li,<sup>ac</sup> Daming Zhuang,<sup>\*ab</sup> Ning Zhang,<sup>c</sup> Ming Zhao,<sup>ab</sup> Xinping Yu,<sup>c</sup> Peng Liu,<sup>c</sup> Yaowei Wei<sup>ab</sup>  
and Guoan Ren<sup>ab</sup>

<sup>a</sup> School of Materials Science and Engineering, Tsinghua University, Haidian District, Beijing, 100084, P. R. China

<sup>b</sup> Key Laboratory for Advanced Materials Processing Technology, Ministry of Education, Tsinghua University, Haidian District, Beijing, 100084, P. R. China

<sup>c</sup> Beijing Sifang Crenergy Optoelectronics Technology Co., Ltd., No. 9, Shangdi 4<sup>th</sup> Street, Haidian District, Beijing, 100085, P. R. China

\*Corresponding author:

Email: dmzhuang@tsinghua.edu.cn

The optimization of the annealing durations of CZTSe absorbers at the selected targeting temperature of 575 °C was conducted with the same process as described in the Experimental section. The annealing durations at temperature of 575 °C were set to be 5 min, 10 min and 20 min. From the SEM images in Fig. S1, the CZTSe grains continuously grow with the increase of annealing durations. However, the images also reveal the increase of amount and size of voids at the grain boundaries.

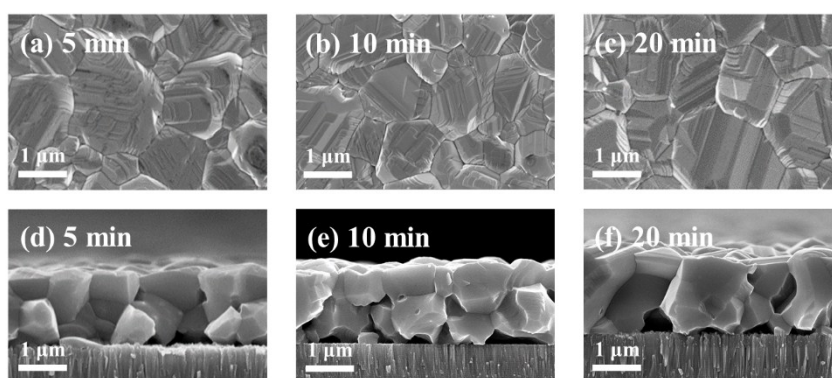


**Fig. S1** (a-c) SEM surface images and (d-e) cross-sectional images of selenized CZTSe absorbers with different annealing durations at temperature of 575 °C. The white bar represents the length scale of 1 μm in the image.

The CZTSe solar cells with the absorbers of different annealing durations were fabricated with the same device structure as described in the Experimental section. Device characteristics were summarized in Table S1. From the results, CZTSe absorbers with annealing duration of 5 min can achieve good-quality of crystallization and high performance of solar cells. As shown in the SEM images, the increase of voids leads the performance degradation. As a consequence, a proper annealing duration of 5 min at the targeting temperature can ensure the solar cells performance.

**Table S1** Average device characteristics of CZTSe solar cells with different annealing durations.

Devices	$V_{oc}$ [mV]	$J_{sc}$ [mA cm <sup>-2</sup> ]	FF [%]	PCE [%]
5 min	415.75	37.27	73.79	11.43
10 min	393.24	37.94	62.87	9.39
20 min	389.92	37.20	55.63	8.08

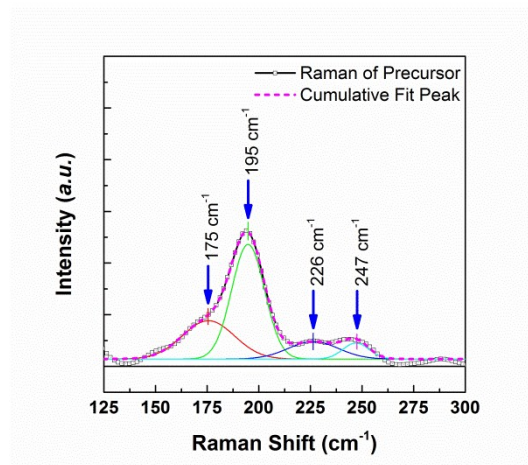


**Fig. S2** Raman spectrum of CZTSe precursor (black line with dot square). Colour lines show the deconvoluted peaks of the Raman spectrum. The short dash line represents the cumulative fit peak of the experimental spectrum. Gaussian line shape is applied in the deconvolution, due to the inhomogeneous broadening of the Raman spectrum for the polycrystalline film.

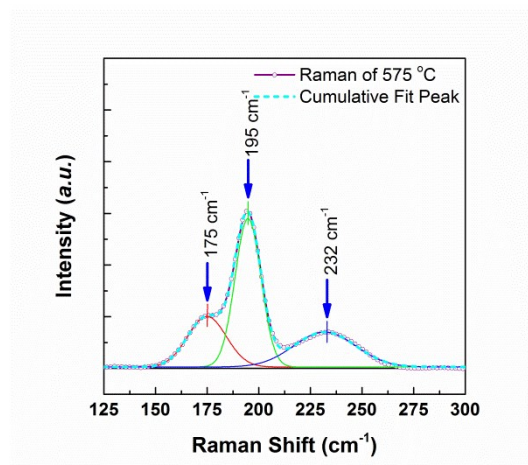


**Fig. S3** Raman spectrum of CZTSe absorber annealed at 575 °C (black line with dot square).

Colour lines show the deconvoluted peaks of the Raman spectrum. The short dash line represents the cumulative fit peak of the experimental spectrum by Gaussian line shape.

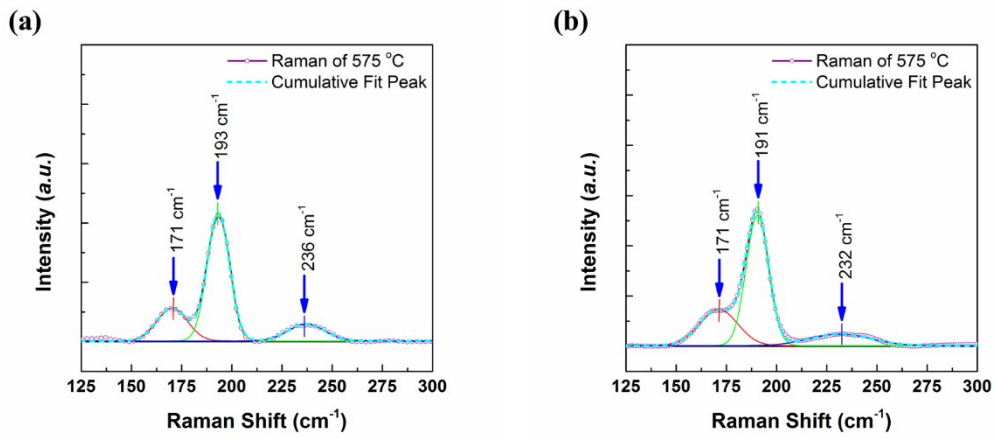


**Fig. S4** Raman spectra with (a) 473 nm and (b) 633 nm lasers excitation of CZTSe absorber annealed at 575 °C (black line with dot square). Colour lines show the deconvoluted peaks of the Raman spectra. The short dash lines represent the cumulative fit peaks of the experimental spectra by Gaussian line shape.

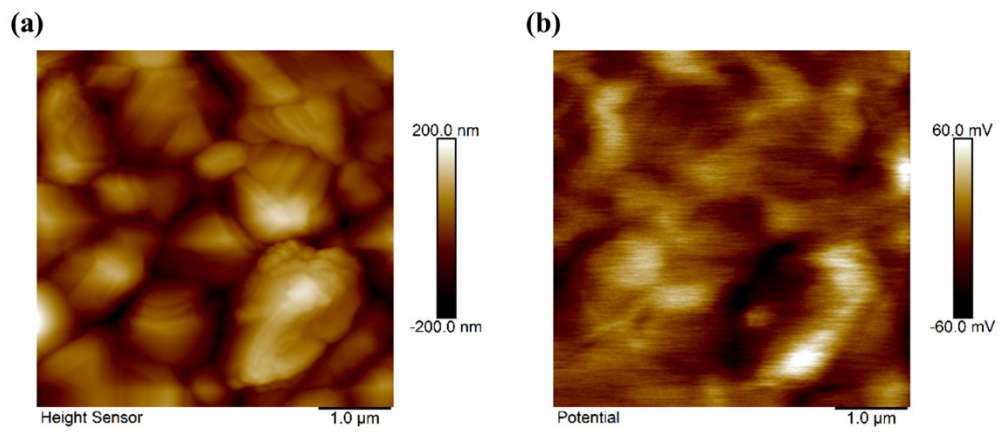


**Fig. S5** The (a) AFM and (b) KPFM images of the CZTSe absorber of annealing temperature of 575

$^{\circ}\text{C}$ .

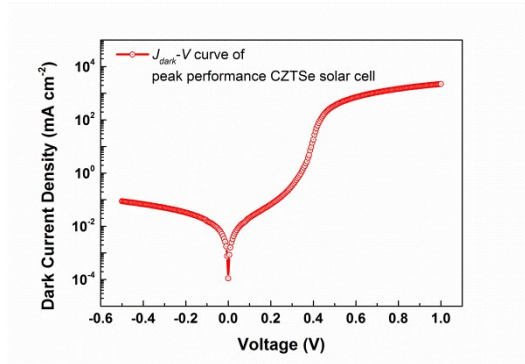


**Fig. S6** The dark current density-voltage ( $J_{dark}$ -V) curve of the peak performance CZTSe solar cell.

The IQE spectrum is given by the equation of

$$IQE(\lambda) = EQE(\lambda) / Absorption(\lambda) . \quad (S1)$$

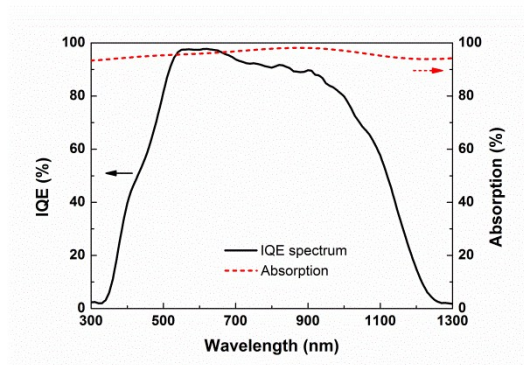


**Fig. S7** The black line and the red dash line represent the IQE and absorption spectra of the CZTSe solar cell, respectively.

The Tauc plot is used to characterize the optical band gap ( $E_g$ ) for semiconductors.<sup>1</sup> For direct band gap material, the band gap can be extrapolated from the intercept with x-axis by linear fitting for  $(\alpha h\nu)^2$  vs.  $h\nu$  in the low energy region. The IQE can be given by

$$IQE \cong 1 - \exp(-\alpha W) \quad (S2)$$

for photon absorption within the depletion-region width  $W$ .<sup>2</sup> The absorption coefficient  $\alpha$  follows the relationship with IQE by

$$\alpha \propto -\ln(1 - IQE). \quad (S3)$$

By plotting  $(h\nu \ln(1 - IQE))^2$  vs.  $h\nu$ , the  $E_g=1.07$  eV can be obtained by fitting the linear part in the low energy region, which is shown in Fig. S8.

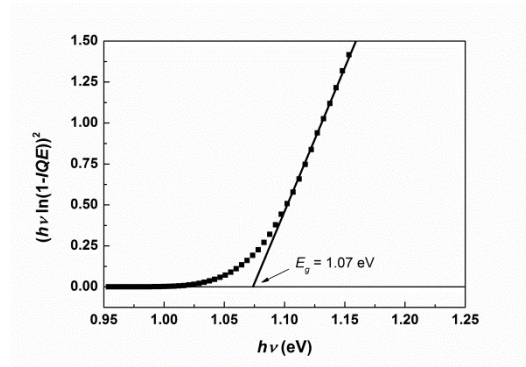


**Fig. S8** The band gap ( $E_g$ ) can be extracted from the plot of  $(h\nu \ln(1 - IQE))^2$  vs.  $h\nu$ .

The Urbach energy ( $E_u$ ) can describe the sub-band gap energy of band tailing states.<sup>3</sup> The absorption coefficient  $\alpha$  below the band gap approximately follows with the relationship of

$$\alpha \propto \exp\left(\frac{(E - E_g)}{E_u}\right). \quad (S4)$$

As the relationship of

$$\alpha \propto -\ln(1 - IQE), \quad (S5)$$

simplified fitting approach can be applied for logarithmic transforming of

$$\ln(-\ln(1 - IQE)) \propto (E - E_g)/E_u \quad (S6)$$

As shown in Fig. S9, the  $E_u=30.3$  meV can be deduced from the slope by linear fitting of  $\ln(-\ln(1 - IQE))$  vs.  $(E - E_g)$  in the energy region lower than 0 eV.

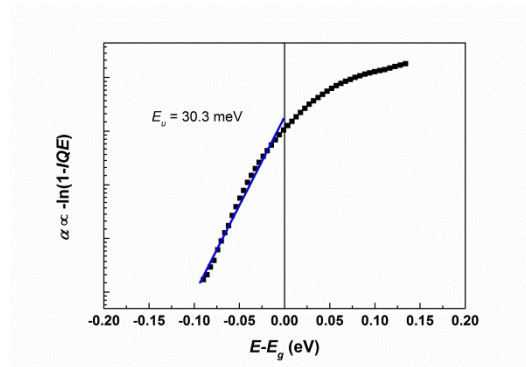


**Fig. S9** The Urbach energy  $E_u=30.3$  meV can be extracted by linear fitting the slope of  $\alpha \propto -\ln(1 - IQE)$  vs.  $(E - E_g)$  plot in the region lower than 0 eV. Note that the ordinate of the plot is given in ln-scale.

Band gap fluctuation of inhomogeneous semiconductors with lateral compositional and phase fluctuations can be described by using a Gaussian distribution module for the band gap  $E_g$  around the mean band gap  $E_{g,mean}$  with a standard deviation  $\sigma_g$ .<sup>4</sup> As the discussion above, the absorption coefficient follows

$$\alpha \propto \sqrt{h\nu - E_g}/h\nu. \quad (S7)$$

The fluctuated absorption coefficient below the band gap can be given as

$$\alpha \propto \int_{-\infty}^{\infty} \frac{1}{\sigma_g \sqrt{2\pi}} \exp\left(-\frac{(E_g - E_{g,mean})^2}{2\sigma_g^2}\right) \frac{\sqrt{h\nu - E_g}}{h\nu} dE_g. \quad (S8)$$

By plotting the curve of  $\alpha \propto -\ln(1 - IQE)$  vs.  $h\nu$ , the fitting curve agrees well with the experimental result. As shown in Fig. 8(a) in the main paper, a standard deviation of  $\sigma_g=35.2$  meV can be extracted from the fitting result.

In situation of electrostatic potential fluctuation, the energy bands are influenced by charged defects induced electrostatic potential. Assuming random distribution of defects, the absorption coefficient below the band gap can be given by the module of Shklovskii and Efros.<sup>5</sup>

$$\alpha \propto \exp\left(-\frac{2}{5\sqrt{\pi}}\left(\frac{2(E_g - h\nu)}{\gamma_{opt}}\right)^{\frac{5}{4}}\right). \quad (S9)$$

In this module,  $\gamma_{opt}$  is used to describe the amplitude of the induced potential fluctuation. After applying logarithmic transforming of  $\ln(\alpha) \propto \ln(-\ln(1 - IQE))$ , exponential fitting result of this module is plotted in Fig. 8(b) in the main paper. An amplitude result of  $\gamma_{opt}=81.6$  meV can be deduced from this result.

## References

1. J. Tauc, *Materials Research Bulletin*, 1968, **3**, 37-46.
2. X. X. Liu and J. R. Sites, *Journal of Applied Physics*, 1994, **75**, 577-581.
3. F. Urbach, *Physical Review*, 1953, **92**, 1324-1324.
4. J. Mattheis, U. Rau and J. H. Werner, *Journal of Applied Physics*, 2007, **101**, 113519.
5. B. I. Shklovskii and A. L. Efros, *Electronic properties of doped semiconductors*, Springer Science & Business Media, 2013.